Pergamon

Int. J. Heat Mass Transfer. Vol. 39, No. 2, pp. 373–382, 1996

0017-9310/96 $9.50+0.00

0017-9310(95)00112-3

Permanent three-dimensional patterns in turbulent flows with essentially two-dimensional wall configurations

S. LORENZ, C. NACHTIGALL and W. LEINER†

Ruhr-Universität Bochum, Institut für Thermo- und Fluiddynamik, 44780 Bochum, Germany

(*Received* 25 *August* 1994 *and in final form* 8 *February* 1995)

Abstract—The phenomenon of steady three-dimensional structures transverse to the main flow direction in turbulent flows with mainly two-dimensional wall configurations has been investigated. Time invariant two-dimensional temperature distributions in an asymmetrically ribbed channel have been detected by infrared thermography and are compared with published data of three-dimensional flow structures in turbulent boundary layers above a single rectangular cavity and a single rib inside a turbulent channel flow, respectively. The periodic length of the observed flow structures corellate quite well among different investigations, although methods of investigation and boundary conditions are different. It can be concluded that such structures in turbulent flows with nearly two-dimensional boundary conditions (large aspect ratio of the cross-section) are self-sustaining flow effects. No physical explanation of the origin of this phenomenon and of the observed dependencies on the wavelength are available yet.

1. INTRODUCTION

Heat transfer at the grooved wall of an asymmetrically ribbed channel in turbulent flow was studied in an earlier paper [1]. The channel was designed with an aspect ratio S/H (span S to clear channel height H) of 20 to provide nearly two-dimensional flow. The grooved wall was heated electrically to provide constant heat flux and its surface temperature distribution was detected by an infrared camera.

Steady periodic temperature patterns across the width of the channel were detected at the bottom of the grooves by Lorenz *et al.* [1] instead of the one-dimensional surface temperature distribution ($\partial T/\partial z = 0$) expected in two-dimensional flow. The authors had not been able to clarify whether the observed two-dimensional temperature patterns were caused by accidental disturbances of the flow, for example by inhomogeneous inflow conditions of the channel, or by self-sustaining permanent periodic three-dimensional flow patterns in the groove.

The phenomenon of time averaged or permanent three-dimensional structures of turbulent channel and boundary layer flows with approximately two-dimensional boundary conditions was detected by Maull and East [2], Kistler and Tan [3], Dimaczek *et al.* [4] and Werner [5]. All of them considered mainly two-dimensional boundary configurations where the flow is characterized by a transverse stagnation line confining a recirculation zone. These investigators studied turbulent flows with inserts by different experimental methods [oil flow visualization and static pressure measurements [2, 3], infrared thermography (IRT) [1], laser-Doppler anemometry (LDA) [4]] or numerical methods [large-eddy simulation (LES) [5]]. However, all of them detected steady three-dimensional flow structures with a permanent periodicity transverse to the main flow. Most of the investigators did not regard three-dimensional structures as their main subject. Consequently they did not make it clear if the observed structures were caused by external disturbances of the flow or if they were generated spontaneously (self-sustained) and merely positioned by small disturbances of the channel wall structure or of the inflow profile.

Steady three-dimensional flow structures in two-dimensional boundaries are well known in laminar flows, e.g. Bénard convection [6], Taylor vortices [7] and Taylor–Görtler vortices [8]. The turbulent fluctuations in turbulent flows damp the driving forces of generation of permanent three-dimensional structures (e.g. centrifugal force for Taylor and Taylor–Görtler vortices) so that these phenomena are rarely observed in turbulent flows.

The earlier results of Lorenz *et al.* [1] detecting steady two-dimensional temperature distributions at the bottom of the groove in an asymmetrically ribbed channel are verified and further investigated in the present study. The main concern is to evaluate typical periodic lengths of such flow structures and their dependencies from the Reynolds number and from geometric parameters. In addition to the study presented in ref. [1] two other different values of the rib to channel height ratio are investigated. The local distribution of the heat transfer coefficient in the flow direction depending on the Reynolds number and on

† Author to whom correspondence should be addressed.

NOMENCLATURE

a	amplitude of Stanton number variation in the z-direction, equation (10)
A	wetted surface area of one rib period [m^2]
b	width of heating module [m]
c_p	specific heat capacity [J kg^{-1} K^{-1}]
C_p	pressure coefficient
d_h	hydraulic diameter, equation (5) [m]
e	rib height and cavity depth, respectively according to Fig. 9 [m]
H	clear channel height [m]
L	periodic length of steady two-dimensional temperature and three-dimensional flow structures in the z-direction, respectively [m]
p	pressure [N m^{-2}]
P	length of one rib period in flow direction [m]
$\dot{q}$	heat flux [W m^{-2}]
Re	Reynolds number, $Re = (\bar{u}d_h)/\nu$
s	rib width and cavity width, respectively according to Fig. 1 [m]
S	total width of channel and cavity respectively, in the z-direction [m]
St_{loc}	local Stanton number, $St_{lok} = \alpha_{lok}/(\rho c_p \bar{u})$
$\overline{St}$	Stanton number averaged transversally to main flow direction
T	temperature [K]
$\bar{u}$	mean flow velocity component in the main flow (x) direction [m s^{-1}]
V	fluid volume within one rib period [m^3]
$\bar{w}$	mean flow velocity component parallel to the rib in the z-direction [m s^{-1}]
x	coordinate in main flow direction [m]
y	coordinate normal to plain channel wall [m]
z	coordinate tangential to plain channel wall, transverse to main flow [m].

Greek symbols

α_{loc}	local heat transfer coefficient [W m^{-2} K^{-1}]
$\bar{\alpha}$	heat transfer coefficient averaged transversally to main flow direction [W m^{-2} K^{-1}]
δ	boundary layer thickness [m]
ζ	wrapped coordinate along the rib contour according to Fig. 2 [m]
ν	kinematic viscosity [m^2 s^{-1}]
ρ	density [kg m^{-3}]
ω	vorticity [s^{-1}].

Subscripts

air	air
fluid	fluid
IRT	measured by infrared thermography
loc	local
max	maximum value
min	minimum value
wall	wall.

the rib to channel height ratio is not considered here (see Lorenz *et al.* [1]).

The relevant studies of steady three-dimensional structures in turbulent flows with nearly two-dimensional boundaries by other investigators are compared with the present experimental results. The aim of this study was to find out if the observed structures are self-sustaining flow phenomena in two-dimensional boundaries or if disturbances by experimental conditions or numerical approaches influence the flows. In the first case of spontaneous generation a more detailed analysis of the phenomenon may help to understand better such steady three-dimensional flow structures in turbulent flows with nominally two-dimensional boundary conditions.

2. LITERATURE REVIEW

Several investigations—experimental and numerical—examine geometrical flow configurations similar to those studied in the present experiments. The common features of these configurations (cf. Fig. 1) are a stagnation line transverse to the main flow limiting a recirculation zone. Detailed informations about the configurations, the parameters investigated and the methods of investigation are given in Table 1. Note that the characteristic length s in the flow direction represents different geometric lengths depending on the geometric configurations considered.

Maull and East [2] examined a turbulent boundary layer above a single rectangular cavity [cf. Fig. 1(a)] of aspect ratio $S/s = 9$ (s is the cavity width) with $Re_\delta = 5 \times 10^4$ at the front corner of the cavity. The width-to-depth-ratio was varied within the range $0.4 \leqslant s/e \leqslant 2$. A non-uniform separation line resembling a regular wave was detected at the bottom of the cavity by an oil flow visualization technique. A reconstruction of the streamlines near the bottom of the cavity is shown in Fig. 2. They measured static pressure at two cross-sections at $x/s = 0.1$ and $x/s = 0.2$, respectively. The detected periodic length (in the z-direction) of the measured C_p-distribution (cf. Fig. 3) and that of the oil pattern are identical.

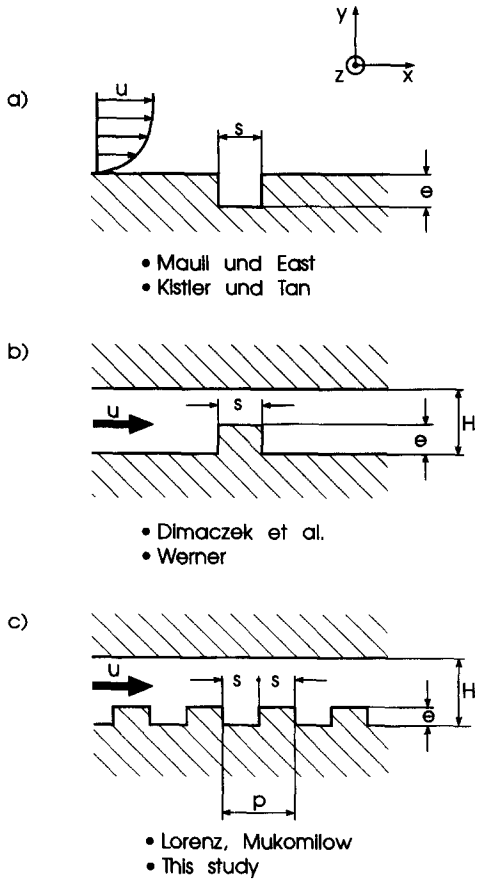

Fig. 1. Two-dimensional wall configurations considered: (a) boundary layer along one single rectangular cavity (Maull and East [2]; Kistler and Tan [3]); (b) channel flow with one single rectangular rib (Dimaczec *et al.* [4]; Werner [5]); (c) channel flow with periodic rib configuration (Lorenz *et al.* [1]; this study).

Maull and East developed an empirical correlation for the periodic length L of the transverse flow structure scaled by the depth e of the cavity valid for all shapes of cavities examined:

$$\left(\frac{L}{e}\right)_{\text{Maull/East}} = 1.2\left(1+\frac{s}{e}\right). \tag{1}$$

The proportion L/e is almost constant for small variations of the Reynolds number of about $\pm 20\%$. The number of periodic cells of the flow depends on the cavity span, whereas L shows a certain variation.

Kistler and Tan [3] investigated the same configuration as Maull and East. The Reynolds number in their experiments was $Re_\delta = 1.5 \times 10^4$. The cavity of an aspect ratio of $S/s = 4$ varied in the range $0.3 \leqslant s/e \leqslant 6$. Kistler and Tan found wavy-like distributions of the pressure coefficient along the z-coordinate from wall pressure measurements. L/e grew when the relative rib thickness s/e was increased.

Dimaczek *et al.* [4] examined a fully developed turbulent flow of water through a channel with a single transverse rectangular rib, as shown in Fig. 1(b). The aspect ratio of their channel configurations ($0.2 \leqslant s/e \leqslant 2$, $1.33 \leqslant H/e \leqslant 4$) was $S/H \geqslant 16$. The Reynolds number regime was $5 \times 10^3 \leqslant Re_e \leqslant 5 \times 10^4$. A crystal violet flow visualization technique yielded steady two-dimensional near-wall flow structures, periodic in the (transverse) z-direction, on the top of the rib, on the front flank, and upstream of the front flank up to a streamwise distance of $1.5 \cdot e$ as shown in Fig. 4. Velocity measurements by means of LDA yielded a wavy-like distribution of the time averaged (transverse) $\bar{w}$ velocity component in the z-direction (cf. Fig. 5). Dimaczek *et al.* did not give a definite value of the proportion $\bar{w}/\bar{u}$, but a peak value of $\bar{w}/\bar{u}$ of ≈ 0.2 can be estimated from their figures. The periodic length L does not change with Re. Dimaczek *et al.* did not present a correlation between the scaled periodic length L/e and the parameter s/e but they stated that L is of the order of $0.4 \cdot (H+e) \leqslant L \leqslant 0.8 \cdot (H+e)$ for all of the configurations investigated.

Werner [5] calculated the velocity field within the wall configuration of Dimaczek *et al.* by LES. Differently from Dimaczek *et al.*, Werner considered one configuration, $s/e = 1$, $H/e = 1$, at one Reynolds number $Re_e = 4.25 \times 10^4$. Werner described transverse periodic three-dimensional structures of the time averaged flow on top of the rib, on the front flank, and within $1.5 \cdot e$ upstream of the rib (cf. Fig. 6), which agrees with Dimaczek *et al.* Werner described the periodic length L by

Table 1. Configuration methods of investigation and parameters of different investigators according to Fig. 1

Reference	Configuration	Reynolds number	Aspect ratio	Method of investigation	
Maull and East [2]	$0.4 \leqslant s/e \leqslant 2$	$Re_\delta = 5 \times 10^4$ ($\pm 1 \times 10^4$)	$S/s = 9$	Oil flow visualization	τ
				Wall pressure measurement	C_p
Kistler and Tan [3]	$0.3 \leqslant s/e \leqslant 6$	$Re_\delta = 1.5 \times 10^4$	$S/s = 4$	Wall pressure measurement	C_p
Dimaczek *et al.* [4]	$0.2 \leqslant s/e \leqslant 2$	$5 \times 10^3 \leqslant Re_e \leqslant 5 \times 10^4$	$S/H \geqslant 16$	Crystal violet method	τ
	$1.33 \leqslant H/e \leqslant 4$			LDA	u, v, w
Werner [5]	$s/e = 1$	$Re_H = 4.25 \times 10^4$	$S/H = 4$	LES	u, v, w
	$H/e = 1$				
Present study	$s/e = 2, p/e = 4$	$10^4 \leqslant Re_{2H} \leqslant 10^5$	$S/H = 20, 10$	IRT	α
	$H/e = 2, 4, 6$			Static pressure distribution	C_p

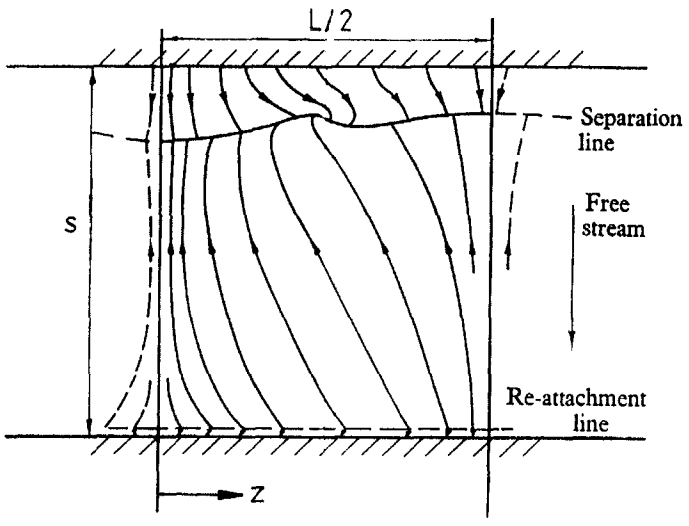

Fig. 2. Reconstruction of streamlines on the bottom of a cavity obtained by oil-film-visualization (Maull and East [2]).

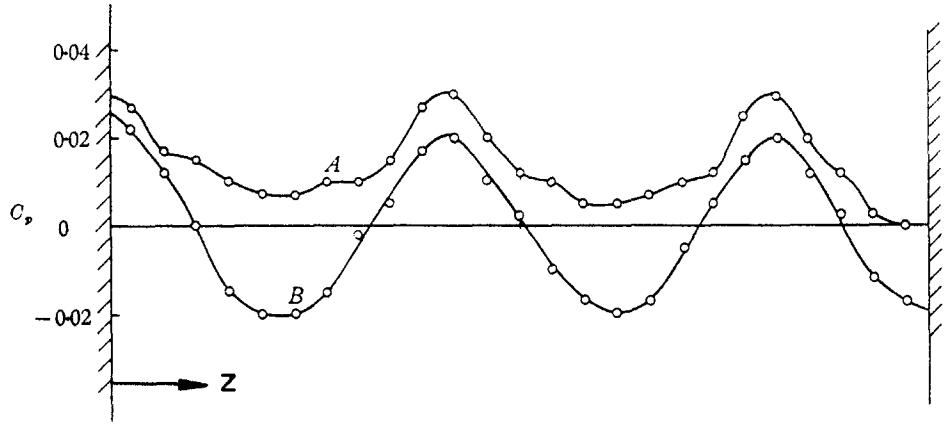

Fig. 3. Static pressure distribution in the z-direction at the bottom of a cavity (Maull and East [2]). (A) $x/s = 0.1$; (B) $x/s = 0.2$.

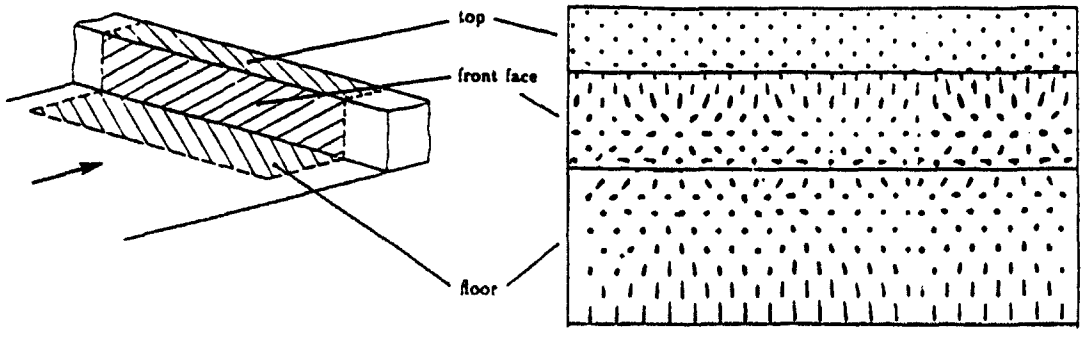

Fig. 4. Flow visualization along the wrapped walls of a single rib (Dimaczec *et al.* [4]).

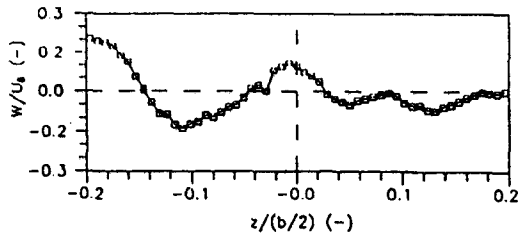

Fig. 5. Time averaged transverse velocity component in the z-direction in front of a single rib (Dimaczec *et al.* [4]).

dence of the scaled transverse periodic length L/e of the flow structure on geometric parameters and on the Reynolds number is consequently not considered principally. Moreover, the authors omit definite statements concerning the 'amplitudes' of the periodic magnitudes. To date, no general overview of investigations on this flow phenomenon is known.

Martinuzzi and Tropea [9] investigated experimentally the flow around three-dimensional cubic obstacles in the same channel as Dimaczek *et al.* They observed horseshoe-like vortices at the front flank of the obstacles and interpreted the periodicity observed

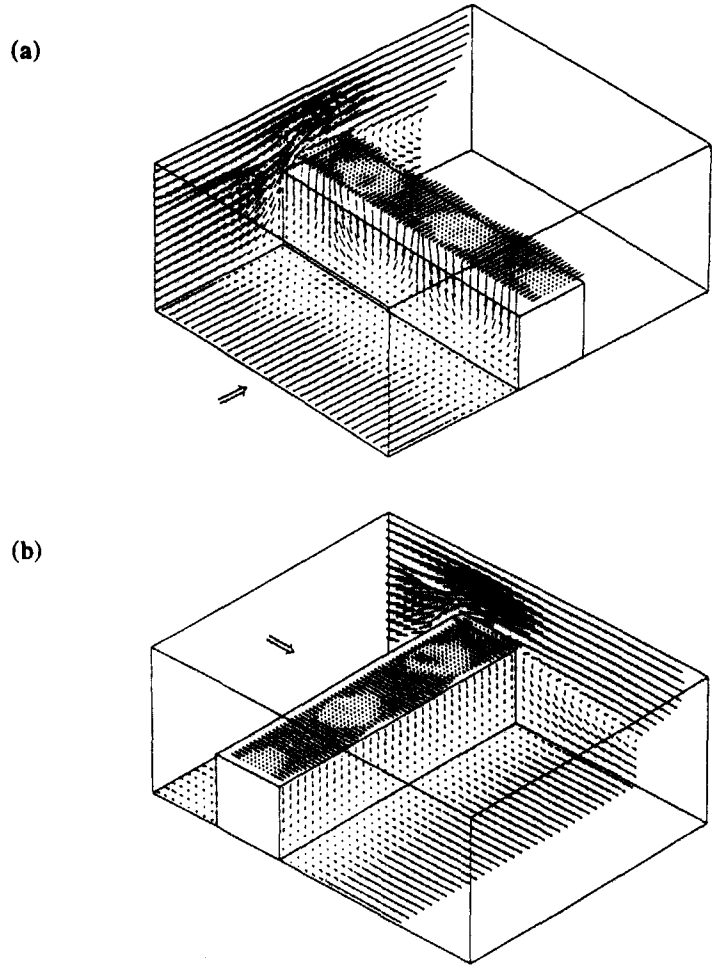

Fig. 6. Time averaged velocity vectors in the first grid plane next to the wall for a single rib from different perspectives (Werner [5]).

$$1.5 \leqslant \left(\frac{L}{e}\right)_{\text{Werner}} \leqslant 2. \qquad (2)$$

He conceded that this value of L/e may have been affected by the periodic boundary condition in the transverse direction combined with a small span ($4H$) of the calculation domain.

The above-mentioned investigations, except the study of Maull and East, mainly consider effects other than three-dimensional flow structures. The dependence by Dimaczek *et al.* similarly to the horseshoe vortices (cf. Fig. 7).

Werner imagined a vortex streak at the front flank, which is bent by the velocity profile over the edge of the rib (cf. Fig. 8), so that an x-component of the vorticity vector exists above the rib and a steady periodic transverse flow structure is generated on top of the rib.

Neither of the models explains sufficiently the physical origin of self-sustaining steady three-dimensional

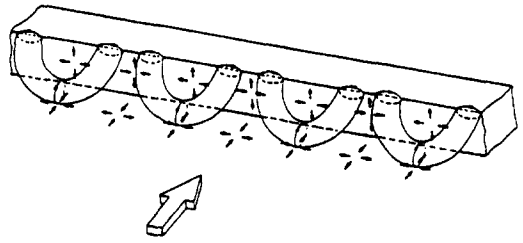

Fig. 7. Model of horse-shoe vortices in front of a single rib causing steady three-dimensional flow (Martinuzzi and Tropea [12]).

$$Re = \frac{\bar{u} d_h}{\nu} \tag{3}$$

is varied in the range $10^4 \leqslant Re \leqslant 10^5$. The hydraulic diameter d_h in equation (3) is defined as

$$d_h = \frac{4V}{A} \tag{4}$$

where V is the fluid volume within one rib period and A is the wetted surface of both walls. The values of the hydraulic diameter are 1.733 H for $e/H = 1/6$, 1.8 H for $e/H = 0.25$ and 2 H for $e/H = 0.5$, respectively.

The local heat transfer coefficient at the ribbed wall of the channel is defined as

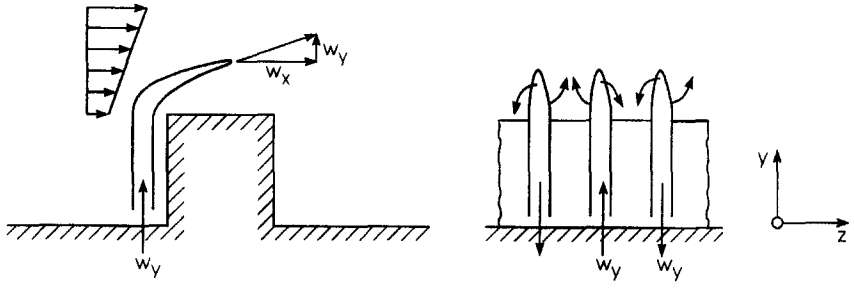

Fig. 8. Model of time history of a single vortex-streak with the vorticity ω causing steady three-dimensional flow (Werner [5]).

flow structures in turbulent flows with essentially two-dimensional boundary conditions.

3. EXPERIMENTAL SETUP AND MEASURING PROCEDURE

Measurements of local heat transfer and wall pressure distribution were carried out within the asymmetrically grooved channel described earlier by Lorenz *et al.* [1] (cf. Fig. 9). With the same ribbed wall configuration of $s/e = 2$ and $p/e = 4$, two different values of clear channel height, $H = 4e$ and $H = 6e$, were investigated in addition to the one ($H = 2e$) examined by Lorenz *et al.* [1]. The aspect ratio is $S/H = 7.5$, 10 and 20, respectively, allowing the channel flow to be considered as nearly two-dimensional. The measuring section is situated downstream of the 27th rib period, where the flow is hydrodynamically periodic. The Reynolds number

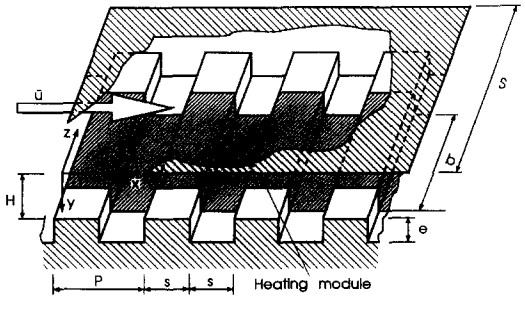

Fig. 9. Periodic rib configuration and geometric magnitudes.

$$\alpha_{loc}(\zeta, z) = \frac{\dot{q}}{T_{wall}(\zeta, z) - T_{fluid}} \tag{5}$$

where T_{fluid} is the mean temperature of the air at the entrance of the considered rib period. Constant wall heat flux is provided by an electric-heating module which is part of the ribbed surface. The heated surface has a span $b = 12 \cdot e$, being one-third of the total span S of the channel (cf. Fig. 9) because of difficulties in manufacturing. The temperature $T_{wall}(\zeta, z)$ at the ribbed contour is measured by IRT. The experimental setup is described in detail in ref. [1].

The bulk temperature T_{fluid} is calculated by an energy balance from the fluid temperature at the entrance of the heated test section and the electric power generated by the heating module along the heated section to the considered rib period (cf. Lorenz *et al.* [1]).

The local Stanton number is defined as

$$St_{loc} = \frac{\alpha_{loc}}{\rho_{air} c_{p\,air} \bar{u}}. \tag{6}$$

The accuracy of temperature measurements was ± 0.3 K and the temperature resolution was 0.07 K. The root mean square error of the local Stanton number as defined by Moffat [10] was about 7%. Static pressure distributions were measured at the bottom of a groove across the channel to detect three-dimensional periodic flow structures assumed to produce the two-dimensional thermal patterns. A series of 37 equidistant pressure tappings of 6.5 mm distance were placed in a line transverse to the main flow at $\zeta/s = 2.6$

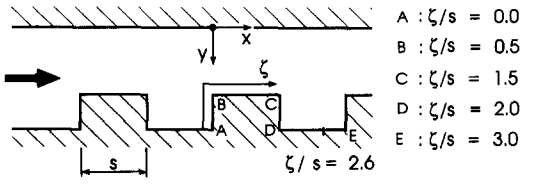

Fig. 10. Longitudinal channel section with definition of coordinate ζ along the ribbed contour.

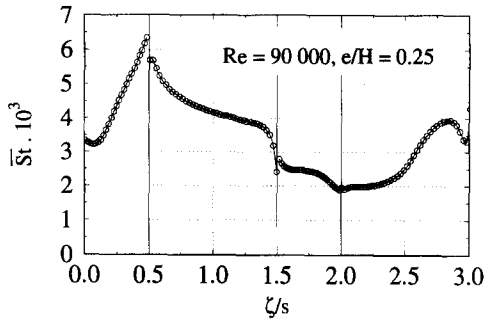

Fig. 11. Transversally averaged Stanton distribution along the ribbed contour ($e/H = 0.25$, $Re_{dh} = 60\,000$).

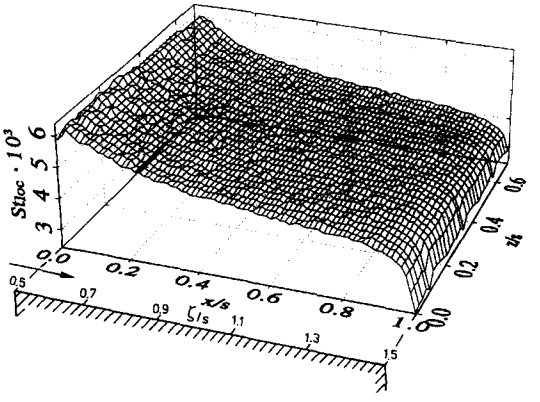

Fig. 12. Two-dimensional Stanton number distribution at the top of the rib ($e/H = 0.25$, $Re_{dh} = 60\,000$).

(cf. Fig. 10), where the contour-coordinate ζ of the ribbed wall is defined by Fig. 10. The position of the tappings was chosen because the local pressure is relatively high there. A scanning valve connects the pressure tappings with a pressure gauge. The dimensionless pressure coefficient C_p is defined as

$$C_p = \frac{2(p - p_{ref})}{\rho_{air}\bar{u}^2} \tag{7}$$

where the reference pressure p_{ref} is the pressure measured at the plane wall just opposite the front flank of the rib at $x = 0$, $y = 0$ (cf. Fig. 10). The accuracy of the measured C_p values is about $\pm 2\%$ of the peak C_p value for $Re \geqslant 50 \times 10^3$ [11].

The absence of any external disturbance that could give rise to the observed structures is to be proved to validate the experiments. In the first stage of experiments measurements by a Pitot-tube proved that the inlet flows from the nozzle was purely two-dimensional. A diffusor fitted at the downstream end of the channel at a distance of $10p$ downstream of the first and $3p$ downstream of the last heated rib period did not cause any detectable disturbance in the test section. The geometric tolerances of the rib configuration were within the accuracy of manufacturing ($\pm 0.005 \cdot e$). External radiation effects were prevented by covering the measuring section from outside by means of a radiation shield. To prove homogenous heating, the heating module was connected for a very short time without any forced convection. The infrared images showed a homogeneous temperature throughout the heating module, which allowed the assumption of good homogenity of heat flux and thermal capacity.

The span of the channel was varied in the regime $3 \leqslant S/H \leqslant 20$ by means of two comb-shaped plates of a length of 10 rib periods, fitted into the grooved channel. These plates were inserted into the measuring section parallelly to the flow at different z-positions to vary the effective span of the channel.

4. RESULTS

The distribution of the Stanton number averaged in the z-direction over $z_2 - z_1 \approx 4e$

$$\overline{St} = \frac{\bar{\alpha}}{\rho_{air} c_{pair} \bar{u}} \qquad \bar{\alpha} = \frac{1}{z_2 - z_1} \int_{z_1}^{z_2} \alpha \, dz \tag{8}$$

and plotted along the dimensionless contour coordinate ζ/s of one rib period is presented in Fig. 11.

The infrared images show, however, that the temperature distribution at the bottom of each heated groove is not one-dimensional (depending on ζ only) for any Reynolds number $Re \geqslant 10\,000$. Steady two-dimensional temperature patterns periodic in the z-direction transverse to the main flow are detected. The temperature differences are about 1.5 K along one groove across the channel. The periodic patterns can only be detected at the bottom of each groove at the contour position $2.0 \leqslant \zeta/s \leqslant 2.2$. The distributions of the local Stanton number of the sixth heated period for $e/H = 0.25$ at $Re = 60\,000$ on the top of the rib and at the bottom of the groove are presented in Figs. 12 and 13, respectively.

From Fig. 13 one can easily recognize a distribution of St_{loc} wavy-like in the z-direction at the upstream side of the bottom of the groove, whereas on the top of the rib (Fig. 12) the distribution is clearly one-dimensional. The local Stanton number at $\zeta/s = 2.1$ varies periodically in the z-direction by approximately 10% for all investigated values of channel height and Reynolds number, see Fig. 14.

$$a = \frac{St_{loc,max} - St_{loc,min}}{St_{loc,min}}. \tag{9}$$

Maxima and minima of the local Stanton number in

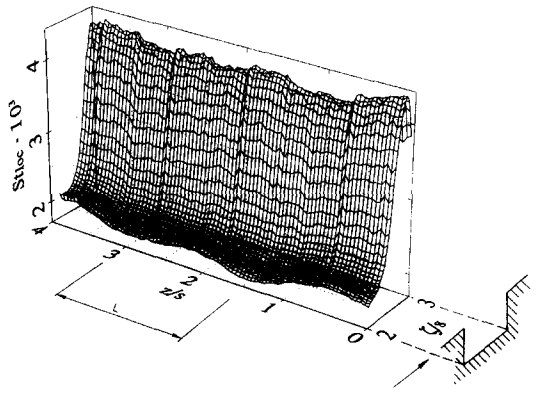

Fig. 13. Two-dimensional Stanton number distribution at the bottom of the groove with the period length L between two temperature maxima ($e/H = 0.25$, $Re_{dh} = 60\,000$).

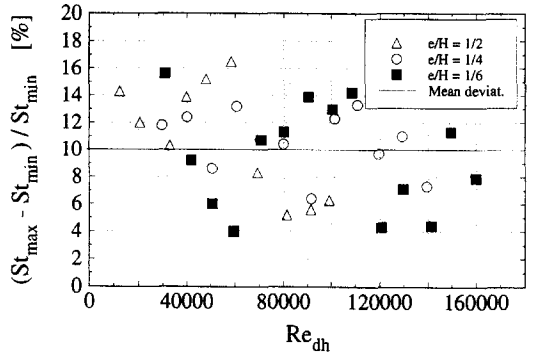

Fig. 14. Relative variation of local Stanton Number in the z-direction vs Re for different clear channel heights.

different grooves are not aligned in the streamwise direction, but they are casually offset in the transverse (z)direction. However, the periodic distances L in the z-direction between two adjacent maxima or two minima of T in one groove are nearly equal for all observed grooves of one configuration. The dimensionless period lengths L/e observed at various Reynolds numbers are of the same order

$$2.8 \leqslant \left(\frac{L}{e}\right)_{IRT} \leqslant 3.3. \qquad (10)$$

The scaled period length L/e does not depend on the Reynolds number. Variation of the free channel height ($e/H = 0.16$, 0.25, 0.5) does not influence L/e either. The influence of the side walls of the channel was investigated by means of the two comb-shaped plates described above. By dislocating these plates in the z-direction the total span of the working section was changed symmetrically and asymmetrically, respectively. In both cases a variation of the aspect ratio within the range $3 \leqslant S/H \leqslant 20$ does not change L/e substantially, but for asymmetrical variation the thermal patterns shift according to the shift of the combs.

Measurements of static pressure distribution were done for the relative rib height $e/H = 0.5$ at $Re = 60\,000$. The transverse distribution of $C_p(\zeta/s = 2.6, z)$ (cf.

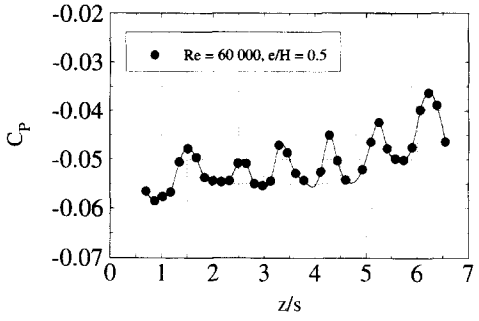

Fig. 15. Static pressure distribution in the z-direction at $\zeta/s = 2.6$ ($x/s = 0.6$) at $Re_{dh} = 110\,000$, $e/H = 0.25$.

Fig. 15) shows a wavy-like character with a 'wavelength' or period length of the order of

$$1.6 \leqslant \left(\frac{L}{e}\right)_{C_p,\zeta/s=2.6} \leqslant 2.6. \qquad (11)$$

The period lengths of heat transfer and pressure distribution, equations (10) and (11), are quite different. Although no evident reason is detectable for this observation it is to be pointed out that the values of periodic length of temperature and pressure distribution, respectively, belong to different (ζ/s)-coordinates with different flow regimes inside the groove. The vortex structure inside the groove observed by flow visualization with helium bubbles [12] is shown schematically in Fig. 16. The periodic lengths $(L/e)_{IRT}$ detected by IRT belong to the regime of the secondary vortex ($\zeta/s = 2.1$), whereas the periodic lengths $(L/e)_{C_p}$ of the C_p measurements were observed underneath the main vortex ($\zeta/s = 2.6$).

5. COMPARISON OF THE PRESENT RESULTS WITH RESULTS OF OTHER INVESTIGATORS

The periodic patterns observed in different investigations are in no case absolutely strict. The presented values of periodic lengths can only be regarded as typical mean values with certain tolerances.

The scaled periodic length L/e found by different authors (cf. Fig. 1) and from the present study are

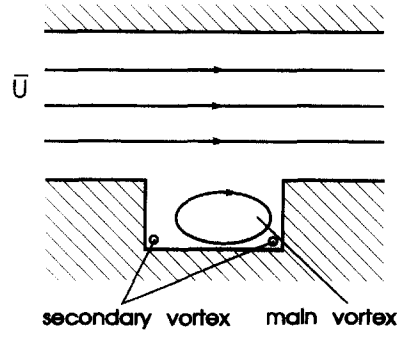

Fig. 16. Schematic diagram of vortex structure inside the groove at $Re_{dh} = 60\,000$, $e/H = 0.5$, from flow visualization by helium filled soap bubbles.

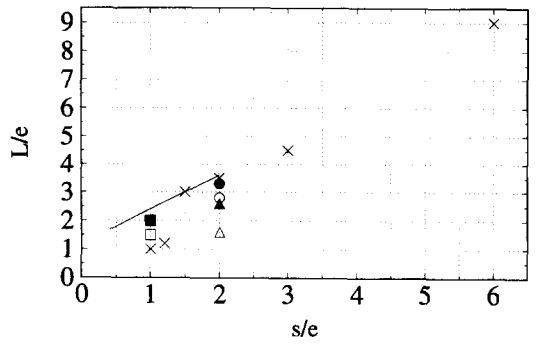

Fig. 17. Scaled period length L/e vs s/e from different investigators [2, 3, 5]; see Table 2.

plotted vs the characteristic geometric proportion s/e in Fig. 17. Note the different definitions of the characteristic lengths s and e according to Fig. 1. Table 2 gives a survey of the relevant details necessary to evaluate the results. The range of L/e given by Dimaczek *et al.* [4] spreads over the whole axis of the diagram; their results therefore cannot be integrated into Fig. 17. The results of the present study [cf. equations (10) and (11)] indicate the possibility that different values of periodic lengths L/e may be efficient at different locations ζ/s of the contour, so that the dependence of L/e on s/e may be ambiguous.

It is conspicuous from Fig. 17 that all period lengths observed are of the same order of magnitude. Despite the different configurations, boundary conditions and methods of investigation of all published data (cf. Fig. 1), the results correspond rather well. The characteristic parameters seem to be the rib height e and the extension of the recirculation zone in the groove with the streamwise length s, respectively. L/e seems to be proportional to s/e for the rib or groove configurations investigated.

The statement that L/e is independent of the Reynolds number and the aspect ratio S/H (see Maull and East [2]) is confirmed by the present study, as Table 2 shows. The present investigation allows one to suppose that the periodic length L/e is independent of the relative rib height e/H.

6. DISCUSSION

Steady three-dimensional flow structures transverse to the main flow have been found by different investigators in the recirculation zones of cavities or in front of single ribs. However, IRT is able to detect periodic thermal patterns attributed to such periodic three-dimensional flow structures in the present experiments only at the bottom of the upstream corner of the groove ($2.0 \leqslant \xi/s \leqslant 2.2$). This is explained as follows: the streamwise velocity $\bar{u}$ is low or close to zero where two-dimensional temperature patterns are observed, whereas the amplitude of the transverse velocity $\bar{w}$ connected to three-dimensional flow effects is of the same order of magnitude through the whole groove. The transverse velocity component $\bar{w}$ influences heat transfer sensibly only when it is of the same order of magnitude as the local streamwise component $\bar{u}$ [$\bar{w}/\bar{u} \approx O(1)$]. This happens in the zone outside of the main vortex (cf. Fig. 16), where two-dimensional temperature patterns were observed ($2.0 \leqslant \xi/s \leqslant 2.2$).

The three-dimensional flow effect described is very important for several disciplines. The time averaged velocity distribution measured in one longitudinal section of a recirculation zone can be different in other parallel sections of equal contour. From this perspective the LDA measurements of Martin and Bates [13] in an asymmetrically ribbed channel in the region just in front of the rib may fail to represent the complete flow field. The knowledge of steady three-dimensional flow structures also has consequences for numerical methods. Werner [5] supposed that the vortex domains near the bottom of the front flank of the configuration of Fig. 9(b) are mostly calculated too large due to the fact that three-dimensionality is suppressed by statistical turbulence models. The periodic lengths of the three-dimensional flow structures in the z-direction are relatively large. This could falsify numerical simulations based on symmetric lateral boundary conditions instead of perioc lateral boundary conditions in grooved channels or when the lateral calculation domain is relatively small.

Several problems exist, in which steady three-dimensional flow structures have some physical effects: the three-dimensional structure probably aug-

Table 2. Legend for results of different investigators according to Fig. 17

Symbol	Reference	Measure	Results
——	Maull and East [2]	$-\tau$	$L/e = 1.2\,(1 + s/e)$
		$-C_p$	$L/e \neq f(Re, S/s)$
×	Kistler and Tan [3]	$-C_p$	$s/e \uparrow \Rightarrow L/e \uparrow$
□ L_{min}	Werner [5]	$-u, v, w$	$1.5 \leqslant L/e \leqslant 2.0$
■ L_{max}			
○ $L_{min,IRT}$		$-\alpha \Rightarrow$	$2.8 \leqslant L/e \leqslant 3.3$
● $L_{max,IRT}$		$-C_p \Rightarrow$	$1.6 \leqslant L/e \leqslant 2.6$
	Present study		
Δ L_{min,C_p}			$L/e \neq f(H/e, B/H \gg 1)$
▲ L_{max,C_p}			$L/e \neq f(Re)$

ments the drag of the flow, which corresponds to a larger pressure drop along the grooved channel. Three-dimensionality influences heat transfer sensibly in regions where local heat transfer coefficients are extremely low. This may produce locally increased thermal stresses, which may be fatal, for example in the cooling of electronic elements.

A more detailed knowledge of the three-dimensional flow structures could be the key to understanding turbulent flows better. These structures are probably produced by instabilities of turbulent flow over mainly two-dimensional obstacles or perturbations. A non-linear theory of stability may be required to describe these turbulent flows.

7. CONCLUSIONS

The observed permanent and periodic two-dimensional temperature and wall-pressure distributions and three-dimensional flow structures in turbulent flows with two-dimensional obstacles are all of the same order of magnitude of wavelength. This leads to the hypothesis that the same physical mechanism is responsible for these different phenomena. The phenomena are probably not caused but merely stabilized by accidential disturbations of the essentially two-dimensional boundary conditions. The transverse velocity component parallel to the ribs reaches values up to $\bar{w}/\bar{u} = 0.2$, whereas the local Stanton number varies for about 10% in the z-direction along the groove.

Extensive parameter studies to clarify the observed dependencies of the wavelength of flow structure from the Reynolds number and the characteristic geometric parameters do not yet exist. A physical model to explain such flow structures and these dependencies is also missing. The phenomenon of transverse periodic flow structures is supposed to be caused by an instability of the turbulent fluctuations sensible to disturbances near the stagnation line. From this assumption, the slightly variable wavelength of the structures can be understood. The observed independence of the wavelength from the Reynolds number can also be explained in this way. If turbulent fluctuations contribute to the three-dimensional steady flow structures, the wavelength is dependent on the degree of turbulence; therefore only a weak dependence on the Reynolds number is to be expected. The Reynolds number variations in the investigations considered here are within one decade, which seems insufficient to identify definitely such a dependence.

REFERENCES

1. S. Lorenz, W. Leiner and D. Mukomilow, Distribution of the heat transfer coefficient in a channel with periodic transverse grooves, *Expl Thermal Fluid Sci.* (1995) (in press).
2. D. J. Maull and L. F. East, Three-dimensional flow in cavities, *J. Fluid Mech.* **16,** 620–632 (1963).
3. A. L. Kistler and F. C. Tan, Some properties of turbulent separated flows, *Physics Fluids* **10,** 165–173 (1967).
4. G. Dimaczek, R. Kessler, R. Martinuzzi and C. Tropea, The flow over two-dimensional, surface-mounted obstacles at high Reynolds numbers, *Proceedings of the Seventh Symposium on Turbulent Shear Flows*, pp. 10.1.1–10.1.6. Stanford University, U.S.A. (1989).
5. H. Werner, Grobstruktursimulation der turbulenten Strömung über eine querliegende Rippe in einem Plattenkanal bei hoher Reynoldszahl, Dissertation, Lehrstuhl für Strömungsmechanik, Technische Universität, München (1991).
6. H. Bénard, Les tourbillons cellulaires dans une mappe liquide, *Rev. Générale Sci. Pures Appl.* **11,** 1261–1271 (1900).
7. G. I. Taylor, Stability of a viscous liquid contained between two rotating cylinders, *Phil. Trans. R. Soc. Lond., Series A*, **223,** 289–343 (1923).
8. H. Görtler, Über eine dreidimensionale Instabilität laminarer Grenzschichten an konkaven Wänden, Nachrichten der Gesellschaft der Wissenschaften, Göttingen, Mathematisch-Physikalische Klasse, Neue Folge, Fachgruppe I, Band 2, pp. 1–26 (1940).
9. R. Martinuzzi and C. Tropea, The flow around surface-mounted, prismatic obstacles placed in a fully developed channel flow, *J. Fluids Engng* **115,** 85–92 (1993).
10. R. J. Moffat, *Describing the Uncertainties in Experimental Results*, Vol. 1, pp. 3–17. Elsevier Science, New York (1988).
11. S. Lorenz, H. Braun, Li Bai and W. Leiner, Wall pressure distribution in a channel with periodic transverse grooves—comparison of experimental and numerical results for turbulent flow, *Proceedings of EUREOTHERM 31, Vortices and Heat Transfer*, pp. 87–92 Ruhr-University, Bochum (1993).
12. S. Lorenz, H. Neumann, K. Schulz and W. Leiner, Evaluation of streamlines and velocities of turbulent airflow by visualization with helium-bubbles. In *Optical Methods and Data Processing in Heat and Fluid Flow*, pp. 111–115. IMechE Seminar Papers, City University, London (1994).
13. S. R. Martin and C. J. Bates, Small-probe-volume laser Doppler anemometry measurements of turbulent flow near the wall of a rib-roughened channel, *Flow. Meas. Instrum.* **3,** No. 2 (1992). Butterworth Heinemann Ltd.